

Reducing Passive Drug Diffusion from Electrophoretic Drug Delivery Devices through Co-ion Engineering

Shao-Tuan Chen[‡], Megan N. Renny[‡], Liliana C. Tomé, Jorge L. Olmedo-Martínez, Esther Udabe, Elise P.W. Jenkins, David Mecerreyes, George G. Malliaras*, Robert R. McLeod* and Christopher M. Proctor*

S.-T. Chen, E. P.W. Jenkins, Prof. G. G. Malliaras, Dr. C. M. Proctor
Electrical Engineering Division, Department of Engineering, University of Cambridge,
Cambridge CB3 0FA, UK
E-mail: gm603@cam.ac.uk, cmp81@cam.ac.uk

M.N. Renny, Prof. R.R. McLeod
Materials Science and Engineering Program, University of Colorado, Boulder, CO 80309,
USA
E-mail: robert.mcleod@colorado.edu

Dr. L. C. Tomé, J. L. Olmedo-Martínez, E. Udabe, Prof. D. Mecerreyes
POLYMAT, University of the Basque Country UPV/EHU, Joxe Mari Korta Center, Avda.
Tolosa 72, 20018 Donostia-San Sebastian, Spain

Prof. D. Mecerreyes
Ikerbasque, Basque Foundation for Science, 48013 Bilbao, Spain

Prof. R.R. McLeod
Department of Electrical, Computer and Energy Engineering, University of Colorado,
Boulder, CO 80309, USA

Keywords: bioelectronics, targeted drug delivery, electrophoretic transport, device optimization

(Abstract

Implantable electrophoretic drug delivery devices have shown promise for applications ranging from treating pathologies such as epilepsy and cancer to regulating plant physiology. Upon applying a voltage, the devices electrophoretically transport charged drug molecules across an ion conducting membrane out to the local implanted area. This solvent-flow-free “dry” delivery enables controlled drug release with minimal pressure increase at the outlet. However, a major challenge these devices face is limiting drug leakage in their idle state. Here, a method of reducing passive drug leakage through the choice of the drug co-ion is presented. By switching acetylcholine’s associated co-ion from chloride to carboxylate co-ions as well as sulfopropyl

acrylate based polyanions, steady-state drug leakage rate was reduced up to 7-fold with minimal effect on the active drug delivery rate. Numerical simulations further illustrate the potential of this method and offer guidance for new material systems to suppress passive drug leakage in electrophoretic drug delivery devices.)

1. Introduction

Electrophoretic drug delivery devices can be implanted directly into the targeted treatment site, bypassing physiological obstacles such as the blood brain barrier^[1] and can achieve higher efficacy while delivering lower dosage compared to systemic administrations.^[2] In contrast to other implantable drug delivery methods such as convection-enhanced delivery devices,^[3] electrophoretic drug delivery does not increase local pressure by injecting solvent, reducing risks of backflow^[4] and issues with long-term device reliability.^[5] Instead of solvent flow, electrophoretic devices use an applied electric field to push drugs across an ion conducting membrane which in turn allows for precise control of the rate of drug delivery and, ideally, a high ratio of drug flow between active and idle states (i.e. ON/OFF ratio). Electrophoretic drug delivery devices encompass a growing family of devices that include different architectures such as the microfluidic ion pump^[6] and the capillary organic electronic ion pump^[7] which have previously shown promise for addressing a wide range of physiological conditions from epilepsy to stress in plants.^[8-13]

Despite this success, limiting drug leakage when the device is idle remains a hurdle to long-term implantation. The flow of drug from the device when it is intended to be OFF could cause side effects or buildup of drug tolerances; not to mention drug leakage reduces the lifetime of the drug source reservoir thereby requiring more frequent refills. Reducing drug leakage is ever more important considering recent advancements in the field that have relied on ever thinner

membranes to reduce power requirements and enhance drug delivery rates.^[6,10,14] Previous attempts to limit diffusive drug leakage for electrophoretic drug delivery devices include increasing membrane resistance,^[15] using a bipolar membrane in a diode configuration rather than a single cation or anion exchange membrane,^[16] increasing the concentration ratio between fixed charge concentration in the membrane to source reservoir, and applying a reverse “retaining” potential during the idle state.^[17] While many of these efforts have proven effective, these solutions increase the energy required to deliver drugs to a therapeutic level thereby reducing the device power efficiency and/or drug delivery rate. Here, we use a combination of experimental work and computational modeling to demonstrate the universal applicability of a new method of reducing drug leakage in electrophoretic drug delivery devices with minimal impact on other performance metrics: changing the drug co-ion in the source reservoir.

The concept of ion pairing has been utilized in drug designs to alter the hydrophilic/hydrophobic balance of drugs molecules.^[18–21] Pairing hydrophilic drug molecules with hydrophobic co-ions/peptides can increase the permeability of drug/co-ion pair into cell membranes,^[22,23] enhance transdermal penetration depth,^[24] or increase the drug solubility.^[25] Ion-pairing can tailor the pharmacokinetics of drugs to different applications without modifying its chemical structure. As a result, this approach increases the chance for regulatory approval and making it a highly attractive method for developing new medications.^[26] For electrophoretic drug delivery devices where drug leakage poses a major challenge for long-term implantation safety and device reliability, the potential of pairing charged drug molecules with different co-ions to reduce the leakage rate has not been previously explored.

In this work, a drug leakage suppression method, termed co-ion engineering, is reported. The theoretical framework describing the relationship between co-ion diffusion coefficient and drug leakage rate from an electrophoretic drug delivery device is presented and validated with

experimental work. Further numerical simulations demonstrate the applicability and consistent leakage reduction capability of co-ion engineering to a variety of drugs commonly used in electrophoretic drug delivery devices. This study shows co-ion engineering can achieve significant drug leakage suppression without sacrificing active device performance or requiring additional operational power. We posit this method can be readily used with a variety of drugs across existing electrophoretic drug delivery devices.

2. Results

2.1. Drug transport mechanisms in an electrophoretic drug delivery device

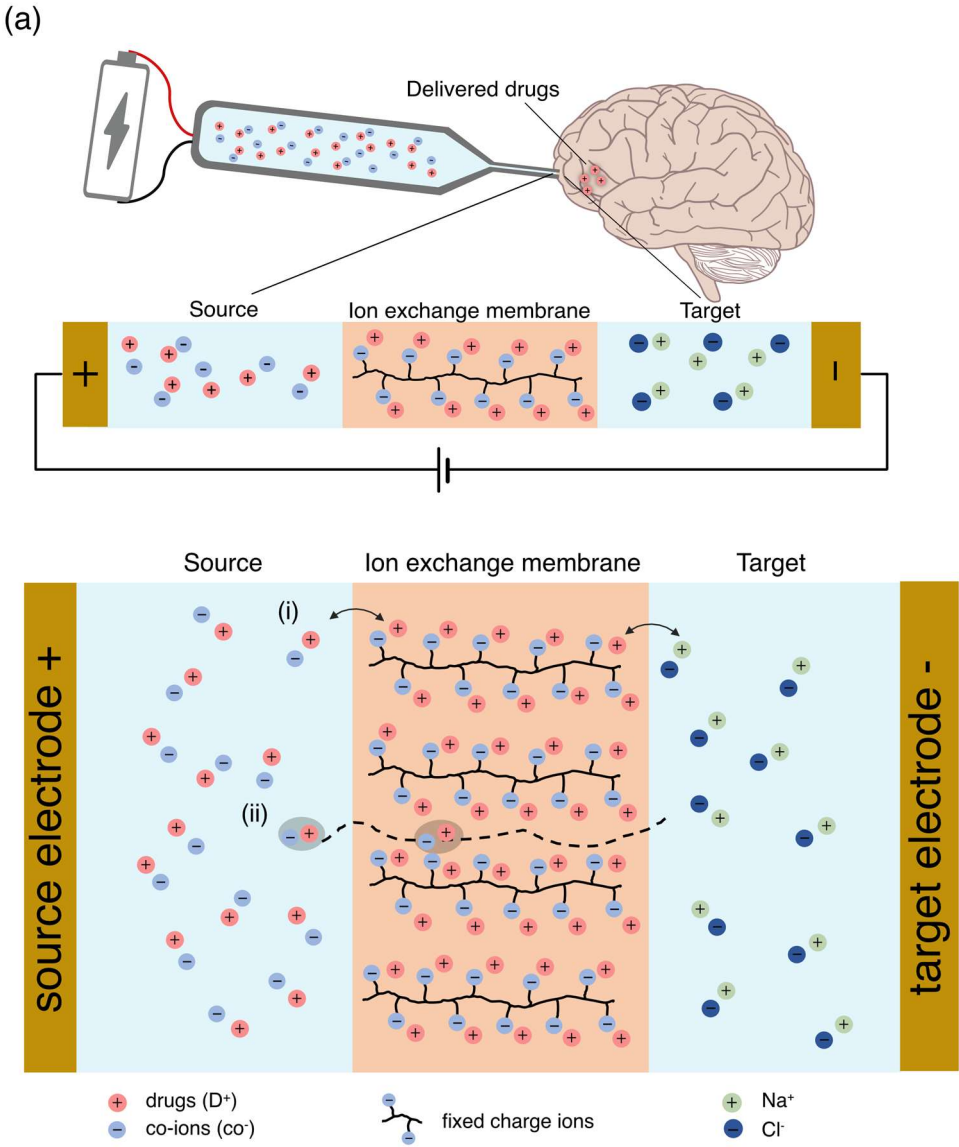


Figure 1. **Working principle of an electrophoretic drug delivery device** (a) Schematic showing different components of an electrophoretic drug delivery device in relation to the implanted area for *in vivo* applications (not to scale). (b) Schematic of mass transport in an electrophoretic drug delivery device. Two drug permeation pathways, (i) Counter-Ion Exchange (IE) and (ii) Associated Ion Diffusion (AID) exist during both active and idle states.

An electrophoretic drug delivery device consists of a source drug reservoir with a source electrode, an ion exchange membrane (IEM) at the point of drug delivery and a target electrode in contact with the target site (e.g. tissue area immediately external to the implant). When the device is in operation, an electric potential is applied between the source and target electrode, transporting the charged drug molecules from the source across the ion exchange membrane and into the target site. The charge of the drug and IEM are chosen deliberately such that the IEM only allows migration of the drug while selectively blocking transport of oppositely charged ions from target back to the source. When the device is idle and no external potential is applied, drug transport across the IEM is significantly reduced however drug leakage across the IEM may still occur due to the concentration gradients between the source, IEM and target.

Drug leakage in an electrophoretic drug delivery device can be understood by analyzing the mass transport mechanisms from the drug source reservoir through the IEM into the target site (Figure 1(b)). The IEM is a polymeric membrane containing fixed charge groups^[27] and in recent years IEMs have been the most commonly reported type of ion conducting membrane used in electrophoretic devices due to their charge selectivity. The IEM separates the drug reservoir, or source, from the target. In both active and idle states, the ionic flux J_i for species i through an IEM of an electrophoretic drug delivery device is described by the one dimensional Nernst-Planck equation along the x -direction as :^[28]

$$J_i = -D_i \left(\frac{da_i}{dx} + \frac{z_i F C_i}{RT} \frac{d\phi}{dx} \right), \quad (1)$$

where D_i is diffusion coefficient, a_i is the activity ($a_i = \gamma_i C_i$), C_i is concentration, z_i is charge number, F is Faraday's constant, R is the gas constant, T is temperature and ϕ is the applied

electric potential. In this study, we take $\gamma_i=1$ and so $a_i=C_i$. In a standard electrophoretic drug delivery device, the high drug activity gradient at the IEM-target interface drives drug out of the membrane and into the target where it is typically metabolized or transported away via convection.^[29,30] The continued loss of drug creates a concentration gradient $\frac{dC}{dx}$ in the membrane, and this concentration gradient is due to irreversible thermodynamic process, regardless of the presence of an external voltage. Reducing this concentration gradient has been the focus of previous reports aiming to limit drug leakage.^[15,31] However, these approaches introduce additional power consumption due to increased ionic resistance. Likewise, reducing the drug concentration in the source reservoir simultaneously reduces the reservoir lifetime as well as the drug delivery rate.^[32]

In this work, we focus on altering the D_i in Equation 1 with the aim of reducing drug leakage without a concurrent effect on power consumption or active drug transport. We hypothesized this may be possible as there are two major pathways for concentration-driven diffusion of charged molecules across an IEM^[33]: ion exchange^[34] (IE) and associated ion diffusion^[35] (AID). In IE, a source counter-ion, which is an ion of opposite charge to fixed-ions, exchanges with a counter-ion that was electrostatically coupled to a fixed-ion in the IEM.^[35] After diffusing across the membrane through IE from fixed-ion to fixed-ion, these counter-ions can once again undergo IE with available counter-ions in the target. The second mechanism, AID, is when a counter-ion dissolves into the membrane as part of a “charge neutral pair” with a co-ion. The ions in this pair are considered associated ions and their transport parameters are coupled. In the absence of an applied electric field, AID is understood to be the primary diffusion mechanism at steady-state for an IEM separating electrolytes of different concentration.^[27,36] Assuming non-ideal thermodynamic factors such as the mismatch in activity coefficients between species in source and target are small,^[37] the overall effective

coupled diffusion coefficient D_s of the charge neutral pair has previously been derived by accounting for electrostatic interactions (counter-ion condensation), tortuosity effect and concentration difference in the IEM.^[38,39] The coupled diffusion coefficient is :

$$D_s = \frac{D_{drug}^m D_{co}^m (C_{drug}^m + C_{co}^m)}{D_{drug}^m C_{drug}^m + D_{co}^m C_{co}^m}, \quad (2)$$

where D_{drug}^m , D_{co}^m , C_{drug}^m , C_{co}^m with superscript m represent the diffusion coefficient and concentration values of drug and co-ions in the IEM.

Considering Equations 1 and 2, it is observed that at steady-state the overall mass transfer of drug due to concentration-driven diffusion in the absence of an applied field is dependent on the diffusion coefficient of the associated co-ions. In theory, one could therefore suppress the drug diffusing from the source reservoir into the target by designing a system with a small co-ion diffusion coefficient. Critically, one would not expect that the co-ion diffusion coefficient would affect drug transport in an applied electric field as such transport primarily occurs via IE and is independent of D_{co} .^[40] With this theoretical basis in mind, we conducted a series of experiments to measure the effect of co-ions on drug leakage.

2.2. Drug leakage profile when paired with co-ions of similar molecular weight

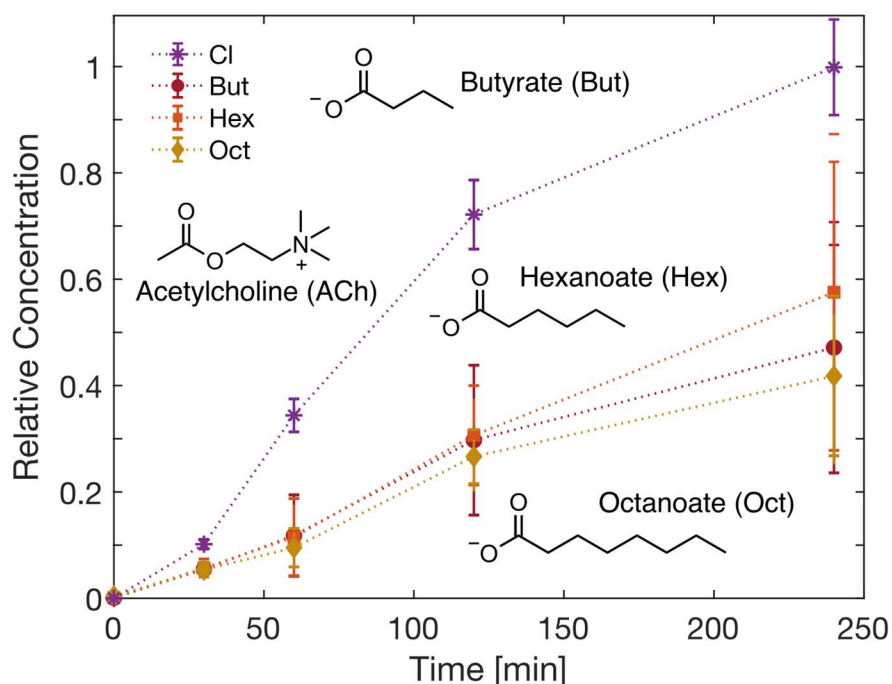


Figure 2. **Time-dependent drug diffusion profile when paired with carboxylate co-ions.** Acetylcholine leakage profile when the source solution was an aqueous electrolyte of Acetylcholine:Carboxylate salt of variable carbon-chain lengths. Inset: molecular structure of Acetylcholine, Butyrate, Hexanoate and Octanoate. Relative concentration is calculated by normalizing against ACh Cl concentration at 240 min.

Acetylcholine (ACh), a drug commonly used in organic electronic ion pumps, was paired with a series of carboxylate co-ions with increasing alkyl chain length, specifically butyrate (But), hexanoate (Hex) and octanoate (Oct) (see Supporting Information Scheme 1). These new acetylcholine salts were prepared by using typical protocols for ionic liquid synthesis (see Supporting Information). Choosing carboxylate as co-ions allow us to adjust the molecular weight by increasing the carbon chain length while avoiding other potential interactions between the drug and co-ions. The goal is to establish the relationship of co-ion diffusion coefficient D_{co} on drug leakage rate from the IEM of an electrophoretic drug delivery device. It is worth remarking that all of salts used in this study are within the family of bioactive ionic liquids based on natural compounds which may have applications in other drug delivery

technologies, where the toxicity of such salts are reported to be negligible for concentration lower than molar ranges^[41-43].

Figure 2 shows the relative ACh concentration measured in the target as a function of time when paired with a series of carboxylate co-ions using a custom-made testing cell with a standard source-IEM-target layout (Figure S1), with acetylcholine chloride as comparison. Measurements were conducted using a polystyrene sulfonate (PSS) based IEM with no externally applied field (see Experimental). For all timepoints the average concentration of diffused ACh was highest for ACh Cl with a roughly 55% reduction in drug leakage observed for the largest co-ion pairing (ACh Oct). However, differences in measured ACh concentration between the carboxylate co-ions were within measurement error (95% confidence interval for at least 3 samples). The results can be understood in terms of D_{co} by employing the modified Stokes-Einstein equation, a power-law relationship between diffusion coefficient D and molecular weight M ($D \propto M^{-\frac{1}{\alpha}}$, $\alpha = 2.56 - 3$).^[44,45] Using this analysis as a first approximation of the relative changes in D_{co} , we estimate a roughly 40% decrease in D_{co} for Oct compared to D_{co} for Cl and a no more than 18% relative reduction in D_{co} when comparing Oct and But co-ions. The results in Figure 2 thus suggest that modest changes in D_{co} can lead to modest changes in drug leakage, and in order to achieve meaningful drug leakage reduction, the change in D_{co} needs to be significant.

2.3. Drug leakage profile when paired with co-ions with orders of magnitude difference in molecular weight

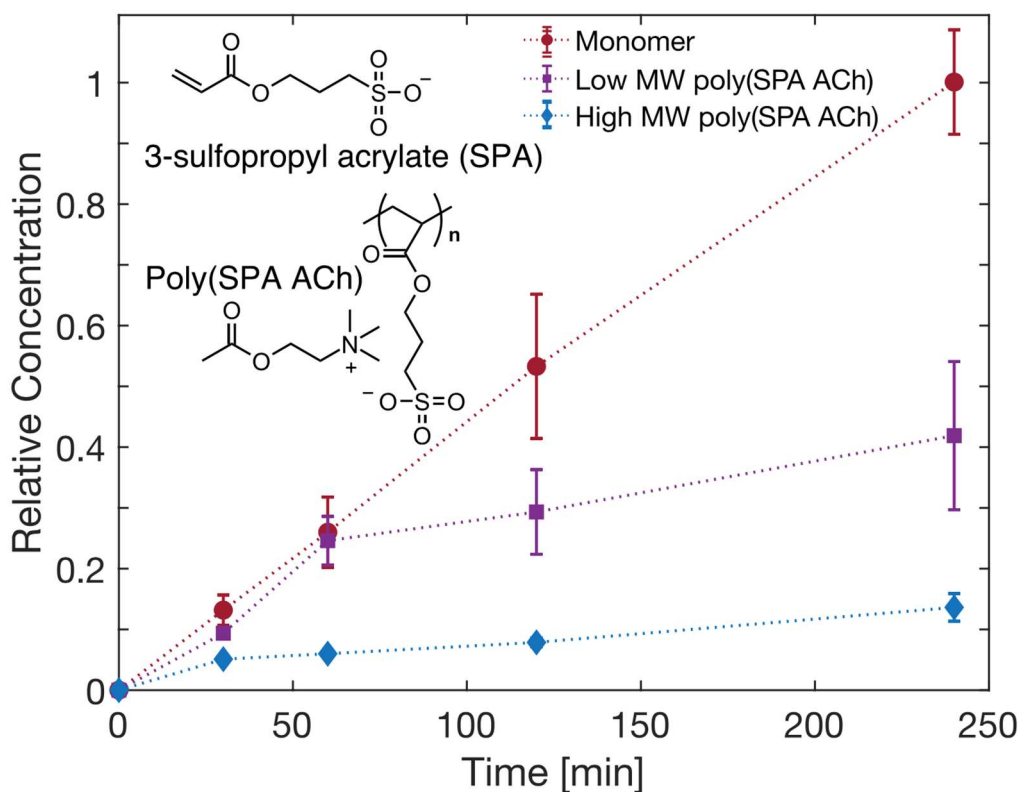


Figure 3. **Time-dependent drug diffusion profile when paired with SPA monomer and polymers.** Acetylcholine time-dependent leakage profile when paired with a series of Acetylcholine:poly(sulfopropyl acrylate)s. Inset: molecular structure of sulfopropyl acrylate (SPA) monomer and polymer. Relative concentration is calculated by normalizing against ACh SPA monomer concentration at 240 min.

To further explore the potential effects of D_{co} on drug leakage, we coupled ACh to polymeric co-ions and performed diffusion experiments. The co-ion of choice, Sulfopropyl acrylate (SPA), was paired with ACh to form the monomer acetylcholine 3-sulfopropyl acrylate (ACh SPA). SPA monomers and polymers are a family of biocompatible compounds suitable to be used in implantable drug delivery applications. SPA polymers have previously been used in biomedical applications including gastro retentive drug delivery systems^[46,47], superporous hydrogel for drug delivery^[48,49], polymer coatings for medical devices^[50,51], and implantable concentration gradient driven power sources for bioelectronics.^[52] By synthesizing polyanion forms of the monomer ACh SPA through free radical polymerization and inverse emulsion (see Supporting

Information for further synthetic procedures), we prepared poly(sulfopropyl acrylate) polyanions with ACh as counter-cations and molecular weight on the order of 85,000 g/mol for low MW poly(SPA ACh) and > 1,000,000 g/mol for high MW poly(SPA ACh), respectively. Following the same calculations based on the modified Stokes-Einstein equation, we estimate the D_{co} for low MW and high MW poly(SPA ACh) to be approximately 10~12% and 4~5% to that of the ACh SPA monomer respectively. It should be noted this estimate is applicable to diffusion in a solvent and, though the IEM is hydrated, it may still significantly underestimate the reduction in diffusion coefficient for polymeric co-ions within the IEM.

Figure 3 shows the relative ACh concentration in the target as a function of time when paired with the ACh SPA monomer, low MW poly(SPA ACh), and high MW poly(SPA ACh) with data points normalized to the ACh concentration with the SPA monomer at 240 minutes. Within 60 minutes, all three samples are observed to approach a constant steady-state rate of acetylcholine leakage. Comparing drug solutions with the three different co-ions, a significant reduction in the steady-state drug leakage rates is observed when ACh was paired with the polymers as co-ions. For the low MW SPA polymer, the steady-state leakage rate was reduced 4-fold, while further switching to high MW SPA polymer resulted in nearly 7-fold reduction in drug leakage compared to the monomeric form of SPA. These findings illustrate the powerful role of the drug co-ion in drug leakage across an IEM in an electrophoretic drug delivery device. A 7-fold reduction could lead to an equivalent extension of the time between re-filling drug solutions. Moreover, drugs typically have a strong dose dependence, so even a 2 -fold reduction in leakage rate could mark the difference between safe operation and undesirable effects.^[53]

2.4. Relation between drug leakage profile and diffusion coefficient via computational modeling

To better understand the role of D_{co} in particular on drug leakage and to explore whether the change in D_{co} can explain the findings presented in Figure 2 and 3, we conducted numerical simulations using our recently reported computational model developed for electrophoretic drug delivery devices.^[32] The one-dimensional model mirrors the geometry of a microfluidic ion pump^[6] with blocking electrode boundary conditions. The temporal behavior of drug leakage was explored with three sets of time-dependent numerical simulations where D_{co} between each run was reduced by an order of magnitude (**Figure 4(a)**) with the D_{drug} and initial D_{co} both equal to D_{ACh} . As in the experimental work, the simulated IEM was loaded with drug at the start of each simulation, causing a higher transient leakage rate as a result of the high initial electrochemical potential gradient. The time-dependent drug leakage profiles demonstrate similar characteristics as shown in Figure 3. The steady-state drug leakage fluxes were found to be 1.1, 0.32 and 0.13 [$\mu\text{M}/(\text{min}\cdot\text{cm}^2)$] from high to low D_{co} solutions by extracting the slope of these three curves from 150 minutes onwards. These results indicate that the steady-state drug leakage rate can be reduced by ca. 3 times and 8 times by reducing D_{co} by one and two orders of magnitude respectively. That these simulations results are on par with the experimental findings in Figure 1(c) supports the notion that the change in D_{co} is the primary reason for the observed reduction in diffusion when comparing ACh with SPA monomer and polymer co-ions.

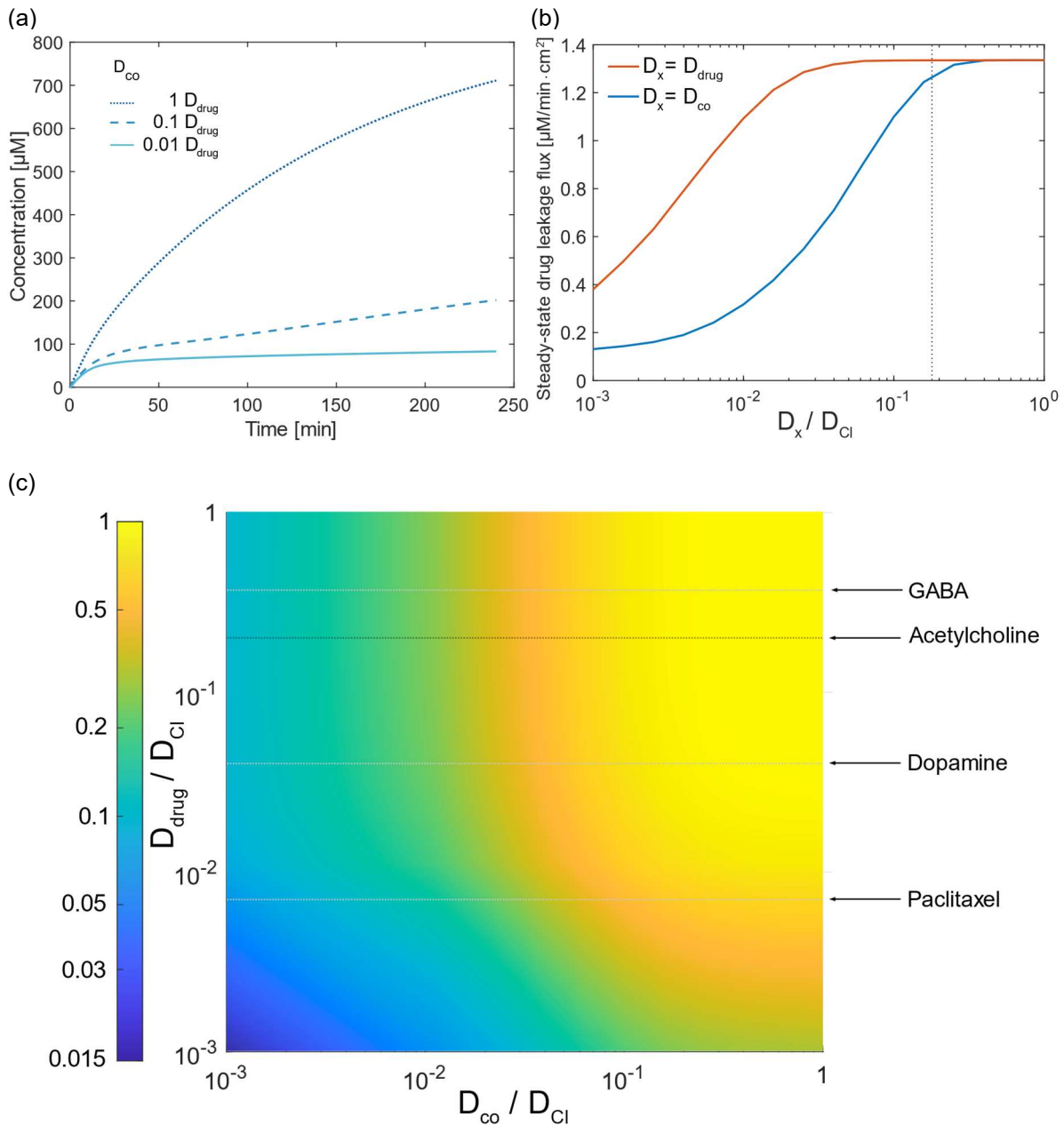


Figure 4. **Numerical simulation results for drug leakage dependence on co-ion diffusion coefficient.** (a) Time-dependent drug leakage profile for different values of D_{co} with D_{drug} fixed as D_{ACh} . (b) Simulation of steady-state drug leakage flux as a function of co-ion (blue line) and drug (orange line) diffusion coefficients. Dotted line represents diffusion coefficient for ACh. (c) Contour plot of steady-state drug leakage as functions of both drug and co-ion diffusion coefficients. Color bar indicates log scale of normalized drug leak rate. Dotted lines represent diffusion coefficient for GABA, ACh, Dopamine, and Paclitaxel.

Having observed the importance of D_{co} in steady-state drug leakage, numerical simulations were further employed to explore a wider range of diffusion coefficient considering both D_{co} and D_{drug} . Figure 4(b) shows the steady-state drug leakage rate for two systems where D_{co} and

D_{drug} are alternatively fixed at D_{ACh} while the other is varied over three orders of magnitude relative to D_{Cl} . The leakage rate is observed to depend strongly on D_{co} (blue line) in the range of roughly 10^{-2} to $10^{-1} D_{Cl}$. A pronounced saturation in drug leakage rate is observed as D_{co} decreases to $10^{-3} D_{Cl}$ and likewise as D_{co} increases above D_{ACh} (noted by dotted line). In contrast, steady-state drug leakage rate is remarkably independent of D_{drug} across nearly two orders of magnitude with a significant decrease starting only when as D_{drug} falls below roughly $10^{-2} D_{Cl}$ (Figure 2(b), orange line). Extending the simulations to consider simultaneous changes in D_{co} and D_{drug} indicates a similar dependence between D_{co} and steady-state drug leakage for D_{drug} ranging from 1 to $10^{-2} D_{Cl}$ with an even more pronounced reduction in drug leakage as D_{drug} approaches $10^{-3} D_{Cl}$ (Figure 4(c)). For reference, dashed lines indicate values for D_{drug} of commonly used compounds GABA, ACh, Dopamine, and Paclitaxel, a notably larger charged drug that may be possible to deliver in the future with further advancements in the development of IEMs for electrophoresis.^[12,14,54] The contour plot shows the remarkable contrast in the effects of D_{drug} and D_{co} on drug leakage rate persist across the spectrum of relevant diffusion coefficient values; where as a decreasing D_{drug} by a factor of 100 may have a negligible effect on steady-state drug leakage rate, the equivalent reduction in D_{co} could reduce the leakage rate 5-fold. As illustrative examples, for GABA, ACh, Dopamine, and Paclitaxel, the steady-state drug leakage rate when paired the same co-ion are nearly identical for D_{co} ranging from 1 to $10^{-2} D_{Cl}$. These findings can be understood in terms of Equation 2. Due to Donnan exclusion, $C_{co}^m \ll C_{drug}^m$, and therefore a change in D_{Drug} would be effectively cancelled out whereas a reduction in D_{co} would directly reduce the effective coupled diffusion coefficient. It is only when D_{drug} is reduced to a factor similar to the ratio of C_{co}^m / C_{drug}^m that the drug leakage rate is noticeably reduced as well.

From a clinical perspective, the significance of these results translates to the wide applicability and consistent drug leakage suppression ability for the co-ion engineering method. Co-ions with higher molecular weight can be widely applied to a variety of drugs to reduce the drug leakage rate, despite the fact that D_{drug} for these drugs vary over 2 orders of magnitude. Furthermore, since the steady-state drug leakage rate is nearly identical in this regime, the proposed co-ion engineering method is drug-independent. The biocompatible SPA co-ion system shown here can therefore be further used by a range of drugs while achieving the same effect of drug leakage suppression, eliminating the need for future researchers to synthesize different co-ions tailored to drugs used in different applications.

2.5. Active performance for electrophoretic drug delivery devices when ACh is paired with different co-ions

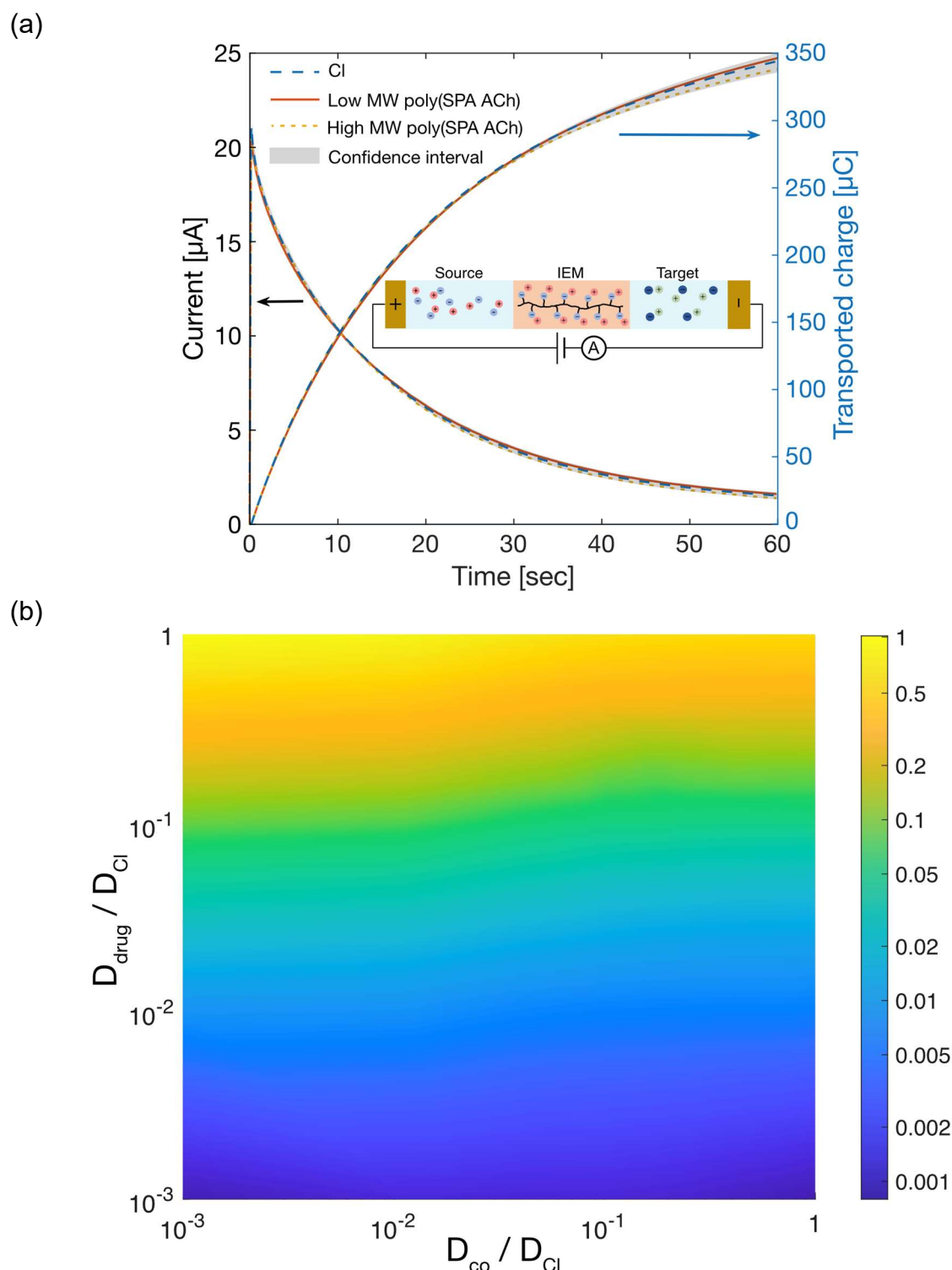


Figure 5. Device performance during active state. (a) Current and charge versus time data for ACh transport by varying co-ions from Cl to high MW SPA polymer (averaged results where $n = 4$ for each co-ion sample). Inset: Circuit connecting scheme for applying constant voltage and measuring the electric current passing through the driving circuit. (b) Contour plot

of active drug transport as functions of both drug and co-ion diffusion coefficient. Color bar indicates log scale of normalized drug delivery rate.

Finally, we investigated how the choice of co-ion affects drug transport with an applied voltage. A microfluidic ion pump device with a PSS based membrane^[6] was prepared with three different 10 mM source solutions of ACh combined with Cl, low MW SPA polymer and high MW SPA polymer co-ions. A 0.5 V potential was applied between source and target electrodes with phosphate buffered saline in the target well (see Experimental). The 0.5V operation voltage was chosen such that it is both within the safety limit for *in vivo* applications^[6,10] and does not introduce additional drug diffusion.^[32,55] Notably, the measured current and transported charge were found to be nearly identical between the three co-ion samples (**Figure 5(a)**). Simulations from our computational model of the microfluidic ion pump further illustrates that active drug transport is largely independent of co-ion diffusion coefficient (Figure 5(b)). Likewise, the simulation shows electrophoretic drug delivery depends strongly on the D_{Drug} with an approximately linear correlation consistent with previously reported experiments.^[17,29,56] The results in Figure 3 follow from established theory of electrophoresis in IEMs – most notably the Nernst-Planck relation and associated expressions for the conductivity of an IEM. Also, according to Marcus Theory for ion pairing,^[40] with the presence of an external electric field, the charged drug is carried across the membrane faster and so the drug salt in the source will dissociate to compensate this unequal loss of drug counter-ion and associated pairs. As a result, IE would be the dominant transport mechanism (see Supporting Information).

These results demonstrate that the drug co-ion can be chosen to minimize drug leakage without affecting the active drug delivery rate. The findings also suggest that a change in binding affinity between ACh and SPA poly-SPA polymer compared to ACh and Cl is unlikely to be a significant contributor to the decreased transport in either the on or off state. (A method for

estimating the ionic strength for a drug with different co-ions can be found in Supporting Information). By the same reasoning, Figure 5(a) indicates that the reduction of drug leakage in the poly (ACh poly-SPA ACh) system cannot be explained by the potential entrapment of ACh molecules in the poly-SPASPA polymer matrix.

3. Discussion and Conclusion

All together the results presented here indicate that drug leakage in IEM based electrophoretic delivery devices can be significantly reduced by coupling drugs to slow moving co-ions. Critically, the use of slower co-ions does not come at the cost of active drug delivery rates nor operational power requirements. Though we focus on anionic co-ions here, the same approach should equally apply to cationic co-ions. As this approach concerns only a change to the drug solution rather than the device geometry, it can be readily integrated into the variety of reported electrophoretic device architectures which to date have relied almost exclusively on the use of drugs with small co-ions such as Cl.^[8,9,12,13,30,56] We posit that that the simulation results in Figure 2(c) may prove particularly useful in guiding future design of new drug co-ion systems with drug leakage rates tailored for the application.

To summarize, we demonstrate, drug leakage in IEM based electrophoretic drug delivery devices can be suppressed without affecting the active device performance by changing the associated co-ion in the drug solution. By way of example, we show that the steady-state leakage rate of acetylcholine can be reduced up to 7-fold by changing its associated co-ion from chloride or carboxylates of increasing alkyl chain length (C4 to C8) to poly(sulfopropyl acrylate). Active drug delivery experiments show that the choice of co-ions in the drug solution does not affect the amount of drug delivered with an applied voltage. Comparing experimental results with numerical simulations, we further demonstrate that the strategy presented in this

paper is compatible with a range of drugs commonly used in electrophoretic drug delivery devices. The simulation results can be used to guide the design of future drug co-ion systems for optimal drug leakage reduction. The method presented here can be readily applied to other electrophoretic drug delivery device architectures thereby extending device lifetime and enabling safe operation for long-term implantations.

4. Experimental Section

1. Membrane Preparation

The membrane was made of over-oxidized polyethyldioxythiophene doped with polystyrene sulfonate (PEDOT:PSS). The PEDOT:PSS was mixed as dodecylbenzyl sulfonic acid [0.1% w/w] from Sigma-Aldrich (Spain), ethylene glycol [5 % w/w] from Fisher Scientific (Spain), and Clevios PH 1000 supplied by Heraeus (Spain) [94.9 % w/w]. To this, 3-glycidmethoxypropyl silane from Sigma-Aldrich was added [1 % w/w]. After 3 minutes of sonication, 250 μ l of this solution was drop cast on Whatman Cyclopore Polycarbonate (Sigma-Aldrich, Spain), track etched membrane with a nominal pore size of 5 microns. The membrane surface was activated by plasma treatment for 150 seconds prior to drop casting. After drying overnight, films soaked for 25 seconds in 3:1 deionized water:Clorox bleach and then rinsed in deionized water. Films were measured to be about 4.3 microns thick.

2. Electrolyte Preparation

The butyric acid (≥ 99 wt% pure), octanoic acid (≥ 99 %), ACh chloride (≥ 99 %), 3-sulfopropyl acrylate potassium salt (KSPA, 96 %), 2,2'-Azobis(2-methylpropionamide) dihydrochloride (AIBA, 97 %), Isopal L (> 90 %), Span 83 (> 60 %) and sodium metabisulfite (SMB, > 99 %) were purchased from Sigma-Aldrich (Spain). The potassium hydroxide (KOH, ≥ 85 %) was supplied by Fisher Scientific (Spain), while hexanoic acid (≥ 99 %) and Softanol 90 were

provided by Acros Organics (Spain) and Quimidroga (Spain), respectively. All these chemicals were used as received. The solvents were of analytical grade and used without further purification.

3. Diffusion Experiments

The test-cell assembly with IEM was placed on a hotplate/stirrer which was set to 25 degrees Celsius and 60 rpm. A stir bar was placed only on the target side reservoir during tests and glass cover slips were used to cover each side to prevent any evaporation. The source side was filled with 2.5 ml of 10 mM ACh electrolyte and the target side was filled with 2.5 ml of phosphate buffered saline solution prepared as suggested. At regular times, the target size cover slip was removed only long enough to collect 200 ul of the target side solution. The level of solution on the target side was always above the port hole in the PDMS gasket for the duration of the experiment so that the mass transfer area of the membrane did not change. Each sample was assumed to be well mixed. Before switching to a new ACh:Anion pair, the membrane was flushed on both sides with deionized water at least five times. All samples were stored in a 4 C refrigerator until assayed for Ach concentration.

4. Colorimetric Assay

A colorimetric assay of ACh was used to quantify the amount of ACh that had diffused into the target via an ACh assay kit [MBS169077] provided by MyBioSource (San Diego, CA, USA). Samples taken from cool storage were centrifuged to ensure accurate sample concentrations. 50 ul of sample were mixed with 100 ul of the 1x Assay Buffer (the provided 10x Assay Buffer diluted to a 10th its concentration) to ensure all samples readings would fall inside the detection range of the kit. As suggested by the kit, 50 ul of these diluted samples were added to a 96 well plate (cellstar) in duplicate which sat on ice to ensure integrity of the samples. Reaction mix was prepared as suggested: Choline Oxidase (25 ul), HRP (10 ul), Colorimetric Probe (100 ul),

and Acetylcholinesterase (20 ul) mixed and diluted with 1x Assay buffer to a total volume of 5 ml in a multichannel pipette reservoir. Standards were also prepared as suggested: 10 ul of the provided Acetylcholine Standard was mixed into 490 ul of the 1x Assay Buffer to obtain the upper bound standard concentration (200 umol). Half the volume of the upper bound was combined with equal volume 1x Assay buffer to obtain a 100 umol standards, and this process was repeated to obtain successive standards of half the previous concentration down to 0.78 umol. Pure 1x Assay Buffer was used to provide the control blank. 50 ul of standards were added to the well plate in quadruplicate. A multichannel micropipette was used to distribute 50 ul of the well-mixed reaction mix to each well, such that each well containing a sample or standard held 100 ul, and the plate was incubated at room temperature for 1 hour away from light.

Finally, the plate was read using a Spectramax ID3 Multi-Mode Microplate Reader (Molecular Devices, San Jose, CA, USA). Again, as suggested, the plate reader was set to read at the 540 nm wavelength. Precision of the assay kit can be examined by referring to figure S3, the Acetylcholine Standard curve which is expected to be a linear relationship between absorbance and ACh concentration. The signal-to-noise ratio of the colorimetric assay varies from 16 dB to 25 dB depending on the ACh concentration of the measured sample.

5. Active Pumping Experiments

Electrophoretic drug delivery devices were prepared according to a previous report^[6]. The devices were loaded with solution consisting of 10 mM ACh paired with either Cl, low MW SPA polymer, or high MW SPA polymer with a phosphate buffered saline solution in the target site. The applied potential was controlled using an Autolab N-series Potentiostat (Metrohm Autolab, The Netherlands) with a custom-designed software interface (Autolab NOVA). The electrophoretic drug delivery device was operated in constant voltage mode, where a DC voltage of 0.5V was applied between the source and target electrodes integrated on the device^[6],

with the circuit connecting scheme shown in the inset of Figure 5(a). The resulting current passing through the driving circuit was recorded by the potentiostat with a sampling rate of 20 Hz. Subsequently, following the previously established protocol,^[8,17,56] transported charge was obtained by integrating the current versus time data. The current measurement has a signal-to-noise ratio > 85 dB when the measured current is above 1 μA .

6. Computational Modeling

The governing equations of the one-dimensional model were solved by Finite Element Method using COMSOL 5.4 software (COMSOL Multiphysics, V5.4, USA). Initial conditions were set where the source reservoir contains both counter-ions and co-ions with concentration of 10 mM, and target reservoir contains 160 mM of NaCl to mimic physiological conditions. Fixed charge concentration in the IEM were set as 0.5M, resulting an IEM with pumping efficiency η of 0.95. For boundary conditions, the electrodes of the electrophoretic drug delivery device were assumed to be perfectly polarizable, with no ionic flux entering or leaving from the electrode surface. No restriction of influx and efflux between electrolyte-IEM interface were imposed on any charged particles considered in the study. For both diffusion and active pumping simulations, final drug concentration in target reservoir was obtained by considering both the influx from IEM to target interface and the integral of drug concentration along the entire length of the target reservoir. Adaptive mesh density scheme was used, where the length of the mesh elements in the bulk of reservoirs were set to be 10^{-10} m, and 10^{-12} m at the electrode-reservoir and reservoir-IEM interfaces to ensure convergence. Diffusion coefficients for charged particles considered in the model are as follow: $D_{\text{Na}^+} = 1.33 \times 10^{-9} \text{ m}^2 \text{ s}^{-1}$, $D_{\text{Cl}^-} = 2.03 \times 10^{-9} \text{ m}^2 \text{ s}^{-1}$, with both D_{drug} and D_{co} varying from 2.03×10^{-9} to $2.03 \times 10^{-12} \text{ m}^2 \text{ s}^{-1}$ with a 0.1 reduction factor for the diffusion coefficient of charged species in the IEM ^[16,27].

Supporting Information

Supporting Information is available from the Wiley Online Library or from the author.

Acknowledgements

STC and MNR contributed equally to this work. STC acknowledges funding from the Cambridge Trust and Ministry of Education, Taiwan. CMP acknowledges funding from the University of Cambridge Borysiewicz Fellowship program as well as the Biotechnology and Biological Sciences Research Council David Phillips Fellowship. LCT has received funding from the European Union's Horizon 2020 research and innovation programme under the Marie Skłodowska-Curie grant agreement no. 745734. EU thanks the Spanish MINECO for her FPU fellowship, while JLOM acknowledges the National Council of Science and Technology (CONACYT) in México for his grant 471837. This work was supported by Marie Skłodowska-Curie Research and Innovation Staff Exchanges (RISE) project under the grant agreement no. 823989 "IONBIKE". MNR acknowledges support from the National Science Foundation grant NSF EMPD 1509909 and NSF Plant Genome Research Project, Special Initiatives grant 1935594.

Received: ((will be filled in by the editorial staff))

Revised: ((will be filled in by the editorial staff))

Published online: ((will be filled in by the editorial staff))

References

- [1] W. M. Pardridge, *NeuroRX* **2005**, *2*, 3.
- [2] Y. H. Bae, K. Park, *J. Controlled Release* **2011**, *153*, 198.
- [3] R. H. Bobo, D. W. Laske, A. Akbasak, P. F. Morrison, R. L. Dedrick, E. H. Oldfield, *Proc. Natl. Acad. Sci. U. S. A.* **1994**, *91*, 2076.
- [4] F. Casanova, P. R. Carney, M. Sarntinoranont, *J. Biomech. Eng.* **2012**, *134*, DOI 10.1115/1.4006404.
- [5] T. Boissenot, A. Bordat, E. Fattal, N. Tsapis, *J. Controlled Release* **2016**, *241*, 144.
- [6] I. Uguz, C. M. Proctor, V. F. Curto, A.-M. Pappa, M. J. Donahue, M. Ferro, R. M. Owens, D. Khodagholy, S. Inal, G. G. Malliaras, *Adv. Mater.* **2017**, *29*, 1701217.
- [7] D. J. Poxson, E. O. Gabrielsson, A. Bonisoli, U. Linderhed, T. Abrahamsson, I. Matthiesen, K. Tybrandt, M. Berggren, D. T. Simon, *ACS Appl. Mater. Interfaces* **2019**, *11*, 14200.
- [8] J. Isaksson, P. Kjäll, D. Nilsson, N. Robinson, M. Berggren, A. Richter-Dahlfors, *Nat. Mater.* **2007**, *6*, 673.
- [9] A. Jonsson, Z. Song, D. Nilsson, B. A. Meyerson, D. T. Simon, B. Linderoth, M. Berggren, *Sci. Adv.* **2015**, *1*, e1500039.
- [10] C. M. Proctor, A. Slézia, A. Kaszas, A. Ghestem, I. del Agua, A.-M. Pappa, C. Bernard, A. Williamson, G. G. Malliaras, *Sci. Adv.* **2018**, *4*, eaau1291.

- [11] M. Seitanidou, R. Blomgran, G. Pushpamithran, M. Berggren, D. T. Simon, *Adv. Healthc. Mater.* **2019**, *8*, 1900813.
- [12] D. J. Poxson, M. Karady, R. Gabrielsson, A. Y. Alkattan, A. Gustavsson, S. M. Doyle, S. Robert, K. Ljung, M. Grebe, D. T. Simon, M. Berggren, *Proc. Natl. Acad. Sci.* **2017**, *114*, 4597.
- [13] I. Bernacka-Wojcik, M. Huerta, K. Tybrandt, M. Karady, M. Y. Mulla, D. J. Poxson, E. O. Gabrielsson, K. Ljung, D. T. Simon, M. Berggren, E. Stavrinidou, *Small* **2019**, *15*, 1902189.
- [14] T. A. Sjöström, A. Jonsson, E. O. Gabrielsson, M. Berggren, D. T. Simon, K. Tybrandt, *Adv. Mater. Technol.* **2020**, *5*, 1900750.
- [15] A. Williamson, J. Rivnay, L. Kergoat, A. Jonsson, S. Inal, I. Uguz, M. Ferro, A. Ivanov, T. A. Sjöström, D. T. Simon, M. Berggren, G. G. Malliaras, C. Bernard, *Adv. Mater.* **2015**, *27*, 3138.
- [16] K. Tybrandt, *Soft Matter* **2017**, *13*, 8171.
- [17] K. Tybrandt, K. C. Larsson, S. Kurup, D. T. Simon, P. Kjäll, J. Isaksson, M. Sandberg, E. W. H. Jager, A. Richter-Dahlfors, M. Berggren, *Adv. Mater.* **2009**, *21*, 4442.
- [18] D. Quintanar-Guerrero, E. Allémann, H. Fessi, E. Doelker, *Pharm. Res.* **1997**, *14*, 119.
- [19] K. D. Ristroph, R. K. Prud'homme, *Nanoscale Adv.* **2019**, *1*, 4207.
- [20] Seung Jin Lee, Sung Wan Kim, *J. Controlled Release* **1987**, *6*, 3.
- [21] P. D. McCrary, P. A. Beasley, G. Gurau, A. Narita, P. S. Barber, O. A. Cojocar, R. D. Rogers, *New J. Chem.* **2013**, *37*, 2196.
- [22] F. Benaouda, M. B. Brown, B. Shah, G. P. Martin, S. A. Jones, *Int. J. Pharm.* **2012**, *439*, 334.
- [23] S.-A. Koufopoulou, C. Pistos, C. Giaginis, A. Tsantili-Kakoulidou, *Int. J. Pharm.* **2006**, *316*, 52.
- [24] J. Arct, M. Chelkowska, K. Kasiura, P. Pietrzykowski, *Int. J. Cosmet. Sci.* **2002**, *24*, 313.
- [25] A. ElShaer, P. Hanson, A. R. Mohammed, *Eur. J. Pharm. Sci.* **2014**, *62*, 124.
- [26] S. Giovagnoli, A. Schoubben, C. Rossi, in *Drug Deliv. Syst. Tuberc. Prev. Treat.*, John Wiley & Sons, Ltd, **2016**, pp. 239–257.
- [27] Y. Tanaka, *Ion Exchange Membranes*, Elsevier, **2015**.
- [28] H. Strathmann, *Ion-Exchange Membrane Separation Processes*, Elsevier, **2004**.
- [29] C. M. Proctor, I. Uguz, A. Slezia, V. Curto, S. Inal, A. Williamson, G. G. Malliaras, *Adv. Biosyst.* **2019**, *3*, 1800270.
- [30] D. Cherian, A. Armgarth, V. Beni, U. Linderhed, K. Tybrandt, D. Nilsson, D. T. Simon, M. Berggren, *Flex. Print. Electron.* **2019**, *4*, 022001.
- [31] A. Jonsson, T. A. Sjöström, K. Tybrandt, M. Berggren, D. T. Simon, *Sci. Adv.* **2016**, *2*, e1601340.
- [32] S.-T. Chen, C. M. Proctor, G. G. Malliaras, *Sci. Rep.* **2020**, *10*, 7185.
- [33] J. Kamcev, M. Galizia, F. M. Benedetti, E.-S. Jang, D. R. Paul, B. D. Freeman, G. S. Manning, *Phys. Chem. Chem. Phys.* **2016**, *18*, 6021.
- [34] F. G. Helfferich, *Ion Exchange*, Courier Corporation, **1995**.
- [35] E. L. Cussler, D. F. Evans, S. M. A. Matesich, *Science* **1971**, *172*, 377.
- [36] J. Kamcev, D. R. Paul, B. D. Freeman, *J. Mater. Chem. A* **2017**, *5*, 4638.
- [37] J. Kamcev, D. R. Paul, G. S. Manning, B. D. Freeman, *J. Membr. Sci.* **2017**, *537*, 396.
- [38] J. Kamcev, D. R. Paul, G. S. Manning, B. D. Freeman, *ACS Appl. Mater. Interfaces* **2017**, *9*, 4044.
- [39] J. Kamcev, D. R. Paul, G. S. Manning, B. D. Freeman, *Macromolecules* **2018**, *51*, 5519.
- [40] Y. Marcus, G. Hefter, *Chem. Rev.* **2006**, *106*, 4585.
- [41] M. Petkovic, J. L. Ferguson, H. Q. N. Gunaratne, R. Ferreira, M. C. Leitão, K. R. Seddon, L. P. N. Rebelo, C. S. Pereira, *Green Chem.* **2010**, *12*, 643.
- [42] É. Szentirmai, N. S. Millican, A. R. Massie, L. Kapás, *Sci. Rep.* **2019**, *9*, 7035.

- [43] H. Liu, J. Wang, T. He, S. Becker, G. Zhang, D. Li, X. Ma, *Adv. Nutr.* **2018**, *9*, 21.
- [44] P. J. Flory, *Principles of Polymer Chemistry*, Cornell University Press, **1953**.
- [45] S. Augé, P.-O. Schmit, C. A. Crutchfield, M. T. Islam, D. J. Harris, E. Durand, M. Clemancey, A.-A. Quoineaud, J.-M. Lancelin, Y. Prigent, F. Taulelle, M.-A. Delsuc, *J. Phys. Chem. B* **2009**, *113*, 1914.
- [46] S. Yang, K. Park, J. G. Rocca, *J. Bioact. Compat. Polym.* **2004**, *19*, 81.
- [47] H. Wen, K. Park, *Oral Controlled Release Formulation Design and Drug Delivery: Theory to Practice*, John Wiley & Sons, **2011**.
- [48] J. Chen, W. E. Blevins, H. Park, K. Park, *J. Controlled Release* **2000**, *64*, 39.
- [49] A. Polnok, J. C. Verhoef, G. Borchard, N. Sarisuta, H. E. Junginger, *Int. J. Pharm.* **2004**, *269*, 303.
- [50] S. F. A. Hossainy, *Biocompatible Polyacrylate Compositions for Medical Applications*, **2015**, US8986726B2.
- [51] J. Stopek, B. Cuevas, J. Hotter, B. Nentwick, A. Irfan, S. Tsai, *Biomaterial Drug Delivery and Surface Modification Compositions*, **2010**, US7850982B2.
- [52] T. B. H. Schroeder, A. Guha, A. Lamoureux, G. VanRenterghem, D. Sept, M. Shtein, J. Yang, M. Mayer, *Nature* **2017**, *552*, 214.
- [53] N. H. G. Holford, L. B. Sheiner, *Clin. Pharmacokinet.* **1981**, *6*, 429.
- [54] C. M. Proctor, C. Y. Chan, L. Porcarelli, E. Udabe, A. Sanchez-Sanchez, I. del Agua, D. Mecerreyes, G. G. Malliaras, *Chem. Mater.* **2019**, *31*, 7080.
- [55] M. Seitanidou, K. Tybrandt, M. Berggren, D. T. Simon, *Lab. Chip* **2019**, *19*, 1427.
- [56] D. T. Simon, S. Kurup, K. C. Larsson, R. Hori, K. Tybrandt, M. Gojny, E. W. H. Jager, M. Berggren, B. Canlon, A. Richter-Dahlfors, *Nat. Mater.* **2009**, *8*, 742.

Supporting Information

Reducing passive drug diffusion from electrophoretic drug delivery devices through co-ion engineering

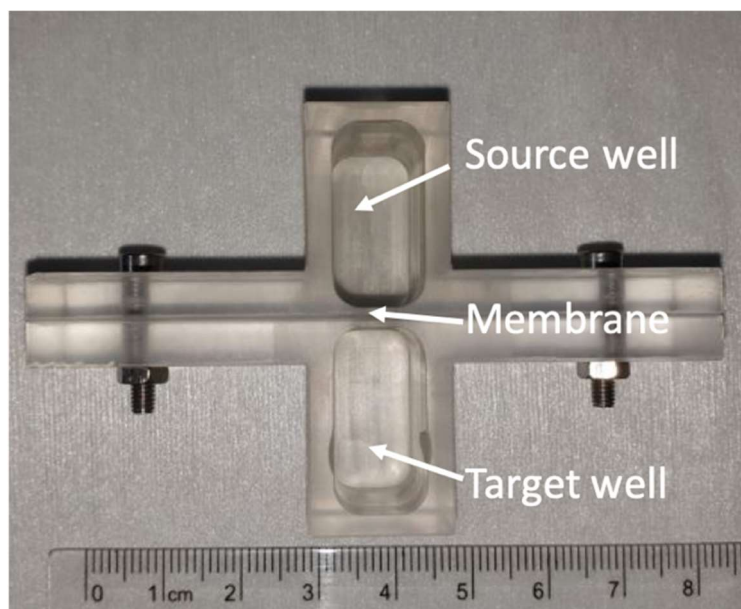


Figure S1. Custom-made test cell for membrane characterization, employed for diffusion experiment in this study.

Synthetic Procedures

Synthesis of ACh Carboxylate Ionic Liquids

ACh-based ionic liquids combining carboxylate anions with variable carbon-chain lengths, including ACh butyrate (ACh But), ACh hexanoate (ACh Hex) and ACh octanoate (ACh Oct), were synthesized *via* a two-step ion exchange method at room temperature (Scheme 1 A). In a typical procedure, potassium hydroxide (0.95 mol) was first dissolved in a minimum amount of water and the desired carboxylic acid (1 mol) was added dropwise. After water removal by rotary evaporation, the obtained precipitate was washed with excess of diethyl ether and filtrated. The formed potassium carboxylate salt (1 mol) and ACh chloride (1 mol) were separately dissolved in a minimum amount of ethanol and then mixed by stirring for 1 hour. The mixture was kept in the freezer overnight to complete the precipitation of KCl, which was then filtered off. After solvent removal by rotary evaporation, the obtained ACh carboxylate

ionic liquids were dried under high vacuum. The chemical structures were confirmed by NMR analysis.

ACh butyrate: ^1H NMR (400 MHz, D_2O): $\delta/\text{ppm} = 4.01$ (m, 2H, OCH_2); 3.47 (t, 2H, NCH_2); 3.16 (s, 9H, $\text{N}(\text{CH}_3)_3$); 2.23 (t, 2H, CH_2COO); 1.96 (s, 3H, CH_3COO); 1.54 (m, 2H, CH_3CH_2); 0.87 (t, 3H, CH_3CH_2). ^{13}C NMR (101 MHz, D_2O): $\delta/\text{ppm} = 181.42$ (CH_2COO); 179.07 (CH_3COO); 67.66 (t, NCH_2); 55.82 (OCH_2); 54.09 (t, $\text{N}(\text{CH}_3)_3$); 37.61 (CH_2COO); 21.99 (CH_3COO); 18.80 (CH_3CH_2); 13.21 (CH_3CH_2).

ACh hexanoate: ^1H NMR (400 MHz, D_2O): $\delta/\text{ppm} = 4.02$ (t, 2H, OCH_2); 3.48 (t, 2H, NCH_2); 3.16 (s, 9H, $\text{N}(\text{CH}_3)_3$); 2.25 (t, 2H, CH_2COO); 1.97 (s, 3H, CH_3COO); 1.54 (m, 2H, $\text{CH}_2\text{CH}_2\text{COO}$); 1.25 (m, 4H, $\text{CH}_3(\text{CH}_2)_2$); 0.83 (t, 3H, CH_3CH_2). ^{13}C NMR (101 MHz, D_2O): $\delta/\text{ppm} = 181.32$ (CH_2COO); 178.82 (CH_3COO); 67.34 (t, NCH_2); 55.53 (OCH_2); 53.80 (t, $\text{N}(\text{CH}_3)_3$); 35.32 (CH_2COO); 30.66 ($\text{CH}_2\text{CH}_2\text{COO}$); 24.62 ($\text{CH}_3\text{CH}_2\text{CH}_2$); 21.68 (d, CH_3CH_2 , CH_3COO); 13.17 (CH_3CH_2).

ACh octanoate: ^1H NMR (400 MHz, D_2O): $\delta/\text{ppm} = 4.02$ (m, 2H, OCH_2); 3.48 (m, 2H, NCH_2); 3.17 (s, 9H, $\text{N}(\text{CH}_3)_3$); 2.14 (t, 2H, CH_2COO); 1.96 (s, 3H, CH_3COO); 1.54 (m, 2H, $\text{CH}_2\text{CH}_2\text{COO}$); 1.25 (m, 8H, $\text{CH}_3(\text{CH}_2)_4$); 0.82 (t, 3H, CH_3CH_2). ^{13}C NMR (101 MHz, D_2O): $\delta/\text{ppm} = 184.01$ (CH_2COO); 173.19 (CH_3COO); 64.51 (t, NCH_2); 58.29 (OCH_2); 53.72 (t, $\text{N}(\text{CH}_3)_3$); 37.41 (CH_2COO); 31.02 ($\text{CH}_2\text{CH}_2\text{COO}$); 28.66 ($\text{CH}_3(\text{CH}_2)_3\text{CH}_2$); 28.23 ($\text{CH}_3(\text{CH}_2)_2\text{CH}_2$); 25.81 ($\text{CH}_3\text{CH}_2\text{CH}_2$), 21.98 (CH_3CH_2), 20.14 (CH_3COO), 13.37 (CH_3CH_2).

Synthesis of poly(sulfopropyl acrylate ACh)

First, the monomer ACh 3-sulfopropyl acrylate (ACh SPA) was prepared (Scheme 1 **B**). ACh chloride (5 g, 27.5 mmol) and 3-sulfopropyl acrylate potassium salt (6.4 g) were previously dissolved in a minimum amount of methanol and then mixed under vigorous stirring at room temperature for 1 hour. A catalytic amount of 4-methoxyphenol was added as an inhibitor and the methanol was stripped off under reduced pressure at temperature ≤ 40 °C. Afterwards, ethanol was added in order to precipitate the KCl, which is a by-product of the anion exchange reaction. The mixture was kept in the freezer overnight to complete the precipitation of KCl. The precipitate was removed by filtration and the excess of ethanol was gently evaporated. Finally, the resulting white solid monomer was thoroughly dried under high vacuum at room temperature for 2 days.

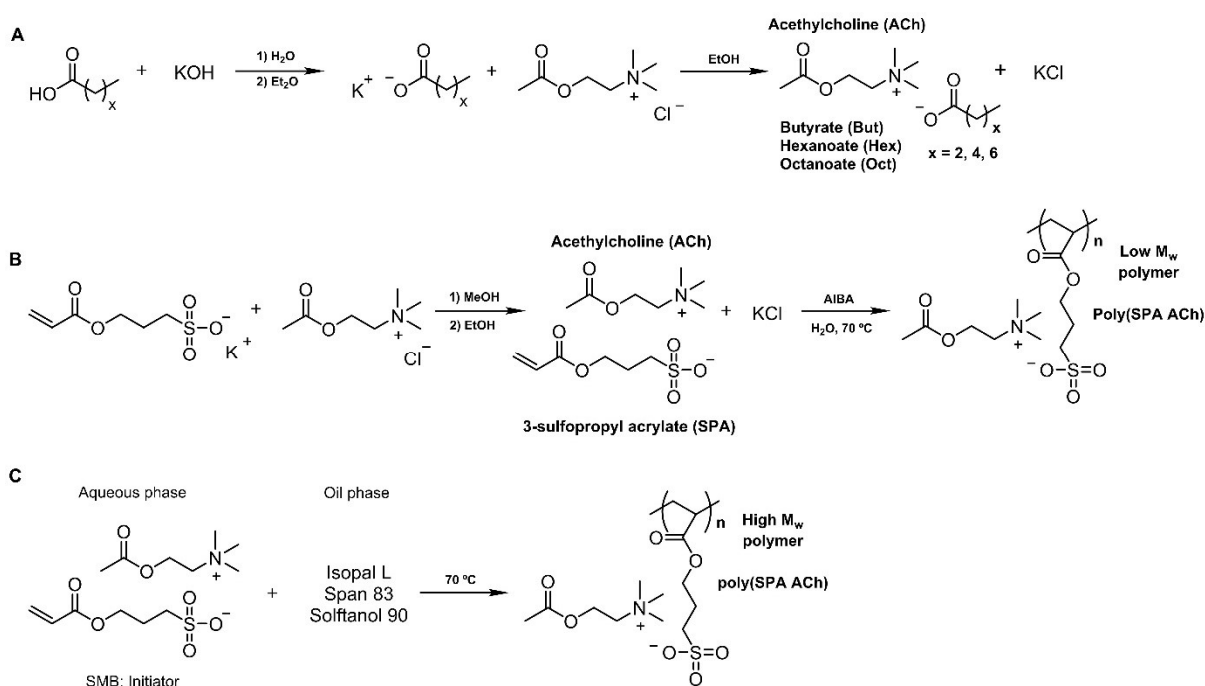
ACh 3-sulfopropyl acrylate: ^1H NMR (400 MHz, D_2O): δ/ppm = 6.47–5.77 (m, 3H, $\text{CH}_2=\text{CH}$); 4.45 (m, 2H, $\text{OCH}_2\text{CH}_2\text{N}(\text{CH}_3)_3$); 4.20 (m, 2H, $\text{OCH}_2(\text{CH}_2)_2\text{SO}_3$); 3.63 (m, 2H, NCH_2); 3.11 (s, 9H, $\text{N}(\text{CH}_3)_3$); 2.92 (m, 2H, CH_2SO_3); 2.12–1.89 (m, 5H, CH_3COO , $\text{CH}_2\text{CH}_2\text{SO}_3$). ^{13}C NMR (101 MHz, D_2O): δ/ppm = 173.14 (CH_3COO); 168.58 ($\text{CH}_2=\text{CHCOO}$); 132.22 ($\text{CH}_2=\text{CH}$); 127.50 ($\text{CH}_2=\text{CH}$); 66.44 (t, NCH_2); 63.52 ($\text{OCH}_2(\text{CH}_2)_2\text{SO}_3$); 58.26 ($\text{OCH}_2\text{CH}_2\text{N}(\text{CH}_3)_3$); 53.68 (t, $\text{N}(\text{CH}_3)_3$); 47.66 (CH_2SO_3); 23.60 ($\text{CH}_2\text{CH}_2\text{SO}_3$); 20.12 (CH_3COO).

The polyanion, poly(sulfopropyl acrylate ACh), i.e. poly(SPA ACh), was synthesized by conventional free radical polymerization in water (Scheme 1 B). In a typical procedure, 2 g of the prepared ACh SPA monomer were dissolved in 18 g of MilliQ water to have a 10 wt% solid concentration. The monomer solution was purged with dry nitrogen for 20 min before being putted into an oil bath at 70 °C. The AIBA initiator (1 wt% to the monomer) was dissolved in water, purged with nitrogen and added dropwise to the monomer solution at 70 °C. The mixture was then allowed to react for 4 h with constant and vigorous stirring. After polymerization, the excess of water was removed by rotary evaporation. The resulting product was then dried under high vacuum at 60 °C for 24 h to remove traces of water and the polyanion was obtained as a white solid.

In order to obtain a very high molecular weight polyanion, the poly(SPA ACh) was also synthesized by inverse emulsion polymerization (Scheme 1 C). The monomer ACh SPA (1.5 g, 4.31 mmol) was dissolved in 0.6 g of water. Isopal L (1.1 g) was used as organic solvent. Span 83 (0.1 g) and Solftanol 90 (0.15 g) were selected as emulsifiers and sodium metabisulfite (SMB) (0.1 g) as initiator. The polymerization reaction was performed at 70 °C for 2 h, under argon atmosphere. The resulting polymer was then precipitated with cold diethyl ether and thoroughly dried under high vacuum at 60 °C for 24 h.

The chemical structures of the synthesized polymers were confirmed by ^1H NMR. The success of the polymerization reaction can be easily seen from the ^1H NMR spectra shown in Figure S2. The signals associated with the acrylic protons between 5.8 and 6.4 ppm of the ACh SPA monomer disappeared after both polymerization reactions, revealing that complete conversion of the monomer was achieved. In addition, the characteristic chemical shifts arising from the 3-

sulfopropyl acrylate polyanion backbone can be clearly observed together with the proton signals associated with the ACh counter-cation. The molar mass of the synthesized polymers was analyzed by SEC/MALS/RI. The equipment was composed by a LC20 pump (Shimadzu) coupled to a miniDawn Treos multiangle (3 angles) light scattering laser and an OptilabT- Rex differential refractometer (all from Wyatt Technology Corp., USA). Separation was carried out using three columns in series (Ultrahydrogel 120, 250, and 2000 with pore sizes of 120, 250, and 2000 Å, respectively, Waters, Barcelona, Spain). The analyses were carried out at 35°C, using a 0.1M LiCl/1.5x10⁻⁵M NaN₃ solution in a mixture of water/acetonitrile (4:1 v/v) at a flow rate of 0.6 ml/min. The refractive index increment was dn/dc= 0.1 ml/g.



Scheme 1: Synthetic pathways for (A) ACh-based ionic liquids combining carboxylate anions, (B) ACh SPA monomer and respective free radical polymerization and (C) inverse emulsion polymerization to form poly(SPA ACh).

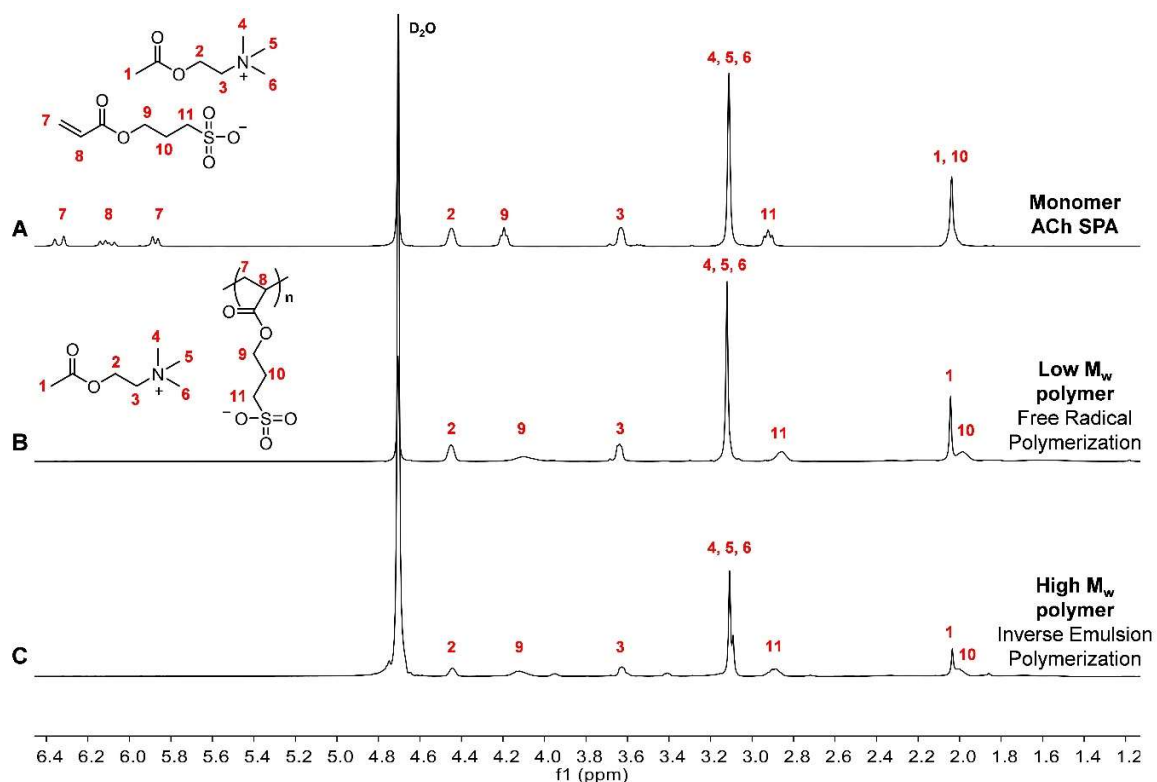


Figure S2. $^1\text{H-NMR}$ spectra of (A) ACh 3-sulfopropyl acrylate monomer, and respective polyanions obtained by (B) free radical polymerization and (C) inverse emulsion polymerization.

Acetylcholine Standard Curves

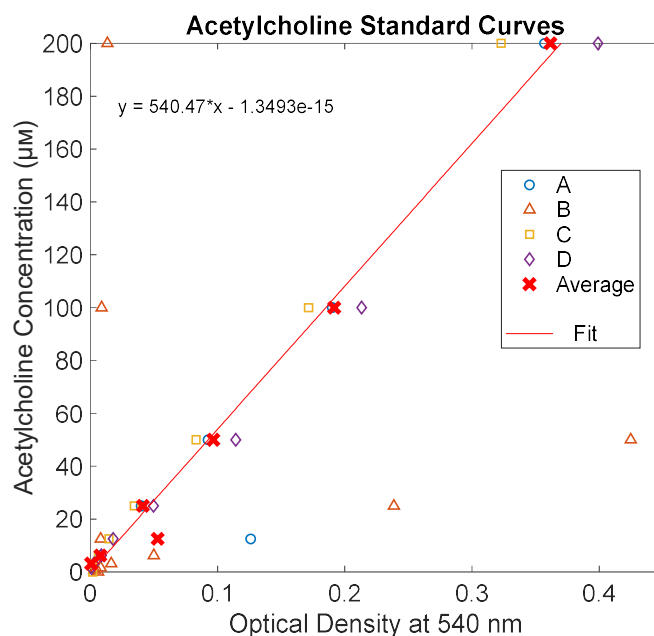
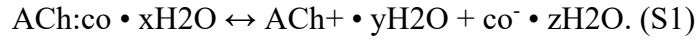


Figure S3. Standard curves used to determine Acetylcholine concentration in samples. Each data series is the same standard solutions placed at 4 different locations in the plate. Series B was not included in the average. The equation is a linear fit to the average where readings using this conversion have an error of 11.2%

Ionic Strength (μ) Consideration:

The drug may spontaneously associate or dissociate with the co-ion in the electrolyte. Such reaction, characterized by changes in hydration sphere necessary to accommodate the different forms, can be written for this process:



The left side of the reaction details the associated form of the drug and the right side of the reaction details the dissociated form. The ratio of dissociated to nominal drug concentrations at equilibrium can be described by the ionic strength, μ .

Marcus Theory for ion pairing states that the energy cost to isolate a multivalent anion from cations is higher than isolating a monovalent anion from the cation. Therefore, in an electrophoretic drug delivery device, the portion of associated ion pairs between ACh and a multivalent high MW SPA polyanion is higher than that of a monovalent chloride system. The ionic strength μ between the drug and co-ion in the electrolyte would dictate the portion between IE and AID pathway.

During active drug pumping, IE is the dominant mass transfer mechanism not only because it is faster due to a larger driving force but because the ratio of dissociated drug remains constant, as dictated by μ , while the total concentration of associated drug diminishes. In the absence of an external electric field, the portion of drug diffusion through IE versus AID for a given drug co-ion system may be proportional to the ionic strength μ of that given system. The total amount of drug diffusion F_{total} through the two mechanisms at steady-state can therefore be written as:

$$F_{total} = \left[\mu D_{drug} \frac{\mu S}{l} + (1 - \mu) D_s \frac{(1-\mu)S}{l} \right], \quad (\text{S2})$$

where S is the solubility coefficient, D_{drug} and D_s is the drug diffusion coefficient and coupled diffusion coefficient between drug and co-ion in the membrane, and l is the membrane thickness.

Membrane conductivity derivation:

The measurement results shown in Figure 3(a) can be understood by relating the measured current to the total ionic flux transported described Nernst-Planck equation.

During drug transport, the total ionic current I with i species is given as:

$$I = F \sum_i z_i J_i, \quad (S3)$$

Plug Equations S3 into the Nernst-Planck equation (Equation 1 in main text), we obtain:

$$I = -\frac{F^2}{RT} \sum_i z_i^2 C_i^m D_i^m \frac{d\psi}{dx}. \quad (S4)$$

The membrane conductivity for an ion exchange membrane is defined as:

$$K = \frac{-I}{\frac{d\psi}{dx}}, \quad (S5)$$

plug in Equations S5 back to Equation S4, the membrane conductivity K can be expressed as a function of the valency, concentration and diffusion coefficient of all the species as:

$$K = \frac{F^2}{RT} (z_{drug}^2 D_{drug} C_{drug} + z_{Co}^2 D_{Co} C_{Co} + z_{Na}^2 D_{Na} C_{Na} + z_{Cl}^2 D_{Cl} C_{Cl}). \quad (S6)$$

Under this framework, changing D_{co} has the least amount of effect on the overall membrane conductivity, since C_{co} is lowest than the rest of the three ions. As a result, further decreasing D_{co} it would not contribute to significant change in membrane conductivity and the amount of transported charge with the same applied voltage.